



Sensitivity of Pliocene Arctic climate to orbital forcing, atmospheric CO₂ and sea ice albedo parameterisation



Fergus W. Howell^{a,*}, Alan M. Haywood^a, Harry J. Dowsett^b, Steven J. Pickering^a

^a School of Earth and Environment, University of Leeds, Woodhouse Lane, Leeds, LS2 9JT, UK

^b Eastern Geology and Paleoclimate Science Center, US Geological Survey, 12201 Sunrise Valley Drive, Reston, VA 20192, USA

ARTICLE INFO

Article history:

Received 8 October 2015

Received in revised form 9 February 2016

Accepted 17 February 2016

Editor: H. Stoll

Keywords:

palaeoclimate

Pliocene

climate model

sea ice

orbital variability

CO₂

ABSTRACT

General circulation model (GCM) simulations of the mid-Pliocene Warm Period (mPWP, 3.264 to 3.025 Myr ago) do not reproduce the magnitude of Northern Hemisphere high latitude surface air and sea surface temperature (SAT and SST) warming that proxy data indicate. There is also large uncertainty regarding the state of sea ice cover in the mPWP. Evidence for both perennial and seasonal mPWP Arctic sea ice is found through analyses of marine sediments, whilst in a multi-model ensemble of mPWP climate simulations, half of the ensemble simulated ice-free summer Arctic conditions. Given the strong influence that sea ice exerts on high latitude temperatures, an understanding of the nature of mPWP Arctic sea ice would be highly beneficial.

Using the HadCM3 GCM, this paper explores the impact of various combinations of potential mPWP orbital forcing, atmospheric CO₂ concentrations and minimum sea ice albedo on sea ice extent and high latitude warming. The focus is on the Northern Hemisphere, due to availability of proxy data, and the large data–model discrepancies in this region. Changes in orbital forcings are demonstrated to be sufficient to alter the Arctic sea ice simulated by HadCM3 from perennial to seasonal. However, this occurs only when atmospheric CO₂ concentrations exceed 300 ppm. Reduction of the minimum sea ice albedo from 0.5 to 0.2 is also sufficient to simulate seasonal sea ice, with any of the combinations of atmospheric CO₂ and orbital forcing. Compared to a mPWP control simulation, monthly mean increases north of 60°N of up to 4.2 °C (SST) and 9.8 °C (SAT) are simulated.

With varying CO₂, orbit and sea ice albedo values we are able to reproduce proxy temperature records that lean towards modest levels of high latitude warming, but other proxy data showing greater warming remain beyond the reach of our model. This highlights the importance of additional proxy records at high latitudes and ongoing efforts to compare proxy signals between sites.

© 2016 Elsevier B.V. All rights reserved.

1. Introduction

The mid-Pliocene Warm Period (mPWP, 3.264 to 3.025 Myr ago, Dowsett et al., 2010) is widely characterised as a period of sustained warmth in Earth's history (Haywood and Valdes, 2004; Haywood et al., 2013), with mean annual temperatures thought to be 2–3 °C higher than the pre-industrial era. Estimates of mid-Pliocene pCO₂ have typically been within the range of 365–415 ppm (Pagani et al., 2010; Seki et al., 2010), but other studies have suggested that it may have been lower, around 270–300 ppm (Zhang et al., 2013; Badger et al., 2013). GCM simulations of the mPWP have not reproduced the magnitude of high-latitude warming of sea surface and surface air temperatures

(SSTs and SATs) indicated by proxy data (e.g. Dowsett et al., 2011; Salzmann et al., 2013). A detailed understanding of forcings which have a strong effect on high latitude climates is therefore important, as their representation in models may have a strong impact on the simulated climates of the past, present and future.

The representation of sea ice in models is one such example. Sea ice can enhance perturbations to the climate via feedback processes such as albedo, in addition to acting as an insulator between the ocean and the atmosphere (Kellogg, 1975; Maykut, 1978; Curry et al., 1995). Previous studies have attempted to reduce the discrepancy between mid-Pliocene high latitude temperature estimates derived from proxy data and model simulated temperatures through reduced sea ice cover. This has been done by artificially removing it year-round in an atmosphere-only simulation (Ballantyne et al., 2013), or by changes to the parameterisation of some sea ice processes (Howell et al., 2014).

* Corresponding author.

E-mail address: eefwh@leeds.ac.uk (F.W. Howell).

Understanding of the state of Arctic sea ice from proxy data in the mid-Pliocene remains limited. Based on the presence of iron grains in marine sediments (located at 87.5°N, 138.3°W), [Darby \(2008\)](#) concludes that the Arctic has had perennial sea ice for the past 14 million years. Analysis of IP₂₅, a sea ice proxy biomarker ([Belt et al., 2007](#); [Brown et al., 2014](#)), in two cores (located at 80.2°N, 6.4°E and 80.3°N, 8.1°E) by [Knies et al. \(2014\)](#) shows that the mid-Pliocene minimum sea ice margin was located to the north of these two sites. [Cronin et al. \(1993\)](#), [Moran et al. \(2006\)](#) and [Polyak et al. \(2010\)](#) show evidence from ostracode assemblages and ice rafted debris that appear to suggest that the mid-Pliocene Arctic sea ice cover was seasonal in nature.

The Pliocene Modelling Intercomparison Project (PlioMIP) has compared the output of the simulation of the mPWP by GCMs from eight different modelling groups ([Haywood et al., 2013](#)). [Howell et al. \(2015\)](#) showed that variability in the ensemble simulation of mid-Pliocene Arctic sea ice is high in the summer months, where four of the models simulate ice-free summers, and the other four, including HadCM3, maintain at least some sea ice coverage year-round.

Model simulations of the mPWP, such as those performed for PlioMIP, typically represent the mid-Pliocene through a fixed atmospheric CO₂ concentration, usually ~400 ppm, and orbital configuration typically identical to modern ([Haywood et al., 2011](#)). However, the mPWP time slab is ~240,000 years long, across which there may have been variations in pCO₂, as well as changes in orbital forcing, which will have affected the state of the Arctic sea ice cover.

This paper focuses on two main issues. It explores the sensitivity of modelled mid-Pliocene Arctic sea ice in HadCM3 to variations in orbital configuration, atmospheric CO₂ concentration and sea ice albedo parameterisation, in isolation as well as in combinations of these factors. In addition, through focusing on those simulations where there is the most extreme reductions in sea ice, this paper investigates the extent to which such large changes can influence the outcomes of data–model comparison, and if they are capable of bringing model and data results into closer agreement.

2. Methods

2.1. Model description

The simulations carried out in this paper were run using HadCM3 (Hadley Centre Coupled Climate Model version 3), a coupled atmosphere–ocean GCM from the UK Met Office. The model incorporates sea ice and vegetation components in addition to the atmosphere and ocean components ([Gordon et al., 2000](#)).

The ocean component contains 20 vertical levels, and has a horizontal resolution of 1.25° × 1.25°, which gives a grid box at the equator of approximately 139 km × 139 km. Vertical levels are distributed to allow greater resolution closer to the surface ([Gordon et al., 2000](#)). The atmosphere component of the model contains 19 vertical levels with a horizontal resolution of 2.5° × 3.75° (latitude × longitude), giving six ocean boxes for every atmosphere grid box. Schemes incorporated in the atmosphere component include a radiation scheme representing effects of minor trace gases ([Edwards and Slingo, 1996](#)), a land surface scheme capable of representing the effects of soil moisture melting and freezing ([Cox et al., 1999](#)) and a gravity wave drag parameterisation ([Gregory et al., 1998](#)).

Parameterisations of ice drift and leads, combined with a basic thermodynamic scheme, are the basis of the sea ice model in HadCM3 ([Cattle and Crossley, 1995](#); [Gordon et al., 2000](#)). The thermodynamic scheme is based on the zero-layer model from [Semtner \(1976\)](#), developed from the one-dimensional sea ice

Table 1

Combinations of orbital configuration (with eccentricity, precession and obliquity values), pCO₂ and minimum sea ice albedo of the 30 simulations. The control simulation is highlighted in bold.

Experiment name	Orbital equivalent (kyr BP)	Eccentricity/precession/obliquity	Atmospheric CO ₂ concentration (ppmv)	Minimum albedo
Mod_300_0.5	Modern	0.016702	300	0.5
Mod_400_0.5		0.01628	400	0.5
Mod_500_0.5		23.439	500	0.5
Mod_300_0.2			300	0.2
Mod_400_0.2			400	0.2
Mod_500_0.2			500	0.2
Jan_300_0.5	3057		300	0.5
Jan_400_0.5		0.053487	400	0.5
Jan_500_0.5		−0.02318	500	0.5
Jan_300_0.2		22.914	300	0.2
Jan_400_0.2			400	0.2
Jan_500_0.2			500	0.2
Mar_300_0.5	3140	0.040574	300	0.5
Mar_400_0.5		0.02343	400	0.5
Mar_500_0.5		22.719	500	0.5
Mar_300_0.2			300	0.2
Mar_400_0.2			400	0.2
Mar_500_0.2			500	0.2
Jul_300_0.5	3037	0.051086	300	0.5
Jul_400_0.5		−0.04239	400	0.5
Jul_500_0.5		23.642	500	0.5
Jul_300_0.2			300	0.2
Jul_400_0.2			400	0.2
Jul_500_0.2			500	0.2
Sep_300_0.5	3053	0.054281	300	0.5
Sep_400_0.5		0.03551	400	0.5
Sep_500_0.5		22.947	500	0.5
Sep_300_0.2			300	0.2
Sep_400_0.2			400	0.2
Sep_500_0.2			500	0.2

model described in [Maykut and Untersteiner \(1971\)](#). Ice dynamics are based on parameterisations described by [Bryan \(1969\)](#). Sea ice advection is derived from the mean current speeds in the top 100 m of the ocean, which are based on windstress in HadCM3 ([Gordon et al., 2000](#)). The parameterisation of sea ice concentration is based on [Hibler \(1979\)](#). For SATs between −10 °C and 0 °C, sea ice albedo is a linear function of the temperature. Albedo is 0.8 at −10 °C and colder, and 0.5 at 0 °C. Salinity of sea ice is constant, at 0.6‰.

2.2. Experimental design

Including the control, thirty simulations of the mid-Pliocene are run. These comprise all combinations of five orbital configurations, three concentrations of atmospheric CO₂, and two minimum sea ice albedo values. These are summarised in [Table 1](#), which also describes the notation used to identify individual simulations. In addition to the mid-Pliocene simulations, a simulation with pre-industrial boundary conditions was also run. Each simulation was run for 500 years, spun off from the same 500 year control run, which was sufficient to ensure all simulations reached an equilibrium state. Climatological averages are based on the last 30 years, and the boundary conditions used are derived from PRISM3D, a reconstruction of mPWP sea surface and deep ocean temperatures, in addition to sea level, topography, vegetation and ice sheet reconstructions ([Dowsett et al., 2010](#)), following the PlioMIP alternate experimental design outlined in [Haywood et al. \(2011\)](#).

2.2.1. Orbital configurations

In addition to the control (orbit identical to modern), simulations of the mPWP were run with four alternative orbital config-

urations. These were selected to test the sensitivity of simulated Arctic sea ice in the mPWP to increased insolation at different times of the year. The four alternative orbits selected were those that, according to the astronomical solution of Laskar et al. (2004), gave the greatest insolation at 65°N in the mPWP during January, March, July and September. January and July were selected due to being the middle months of the traditional definitions of winter (DJF) and summer (JJA) respectively. March and September were selected as Arctic sea ice reaches its maximum and minimum extents respectively in these months. Eccentricity, precession and obliquity values for each orbital configuration are summarised in Table 1.

2.2.2. Atmospheric CO₂ concentrations

Atmospheric CO₂ concentrations of 300 ppm and 500 ppm are used, in addition to the control level of 400 ppm. Whilst some studies have suggested that 300 ppm is a plausible pCO₂ value for the mPWP, or at least for some part of the period (e.g. Zhang et al., 2013; Badger et al., 2013), 500 ppm is greater than the maximum values that have normally been suggested for the mid-Pliocene. The 500 ppm solutions are intended to provide a guide to the sensitivity of the Arctic sea ice to changes in pCO₂, and the state of the Arctic climate under extreme forcings to the sea ice, rather than a simulation of a mid-Pliocene climate that is likely to have existed. CO₂ is only one greenhouse gas, and others such as CH₄ have traditionally been omitted in mid-Pliocene experiments. A pCO₂ value of 500 ppm could therefore provide the overall increase in radiative forcing as a result from CO₂ and other greenhouse gases.

2.2.3. Minimum sea ice albedo

Recent observations have demonstrated that sea ice albedos are generally lower on seasonal sea ice in comparison to multi-year sea ice (Perovich and Polashenski, 2012; Riihela et al., 2013). Howell et al. (2014) suggested that the standard parameterisation of sea ice albedo in HadCM3, with a fixed lower limit of 0.5, may not be appropriate for the mPWP. With a warmer than present climate the Arctic sea ice cover is likely to have consisted of a greater proportion of seasonal sea ice compared to present day. Howell et al. (2014) used parameterisations with alternative lower limits of 0.2, 0.3 and 0.4. The lowest limit of 0.2 is used in the ensemble in this study, along with the control lower limit of 0.5.

2.3. Data analysis techniques

2.3.1. Data–model comparison

This paper uses the same methods as Howell et al. (2014) for the data–model comparison. Proxy data temperature estimates for SATs are based on palaeobotanical data (Salzmann et al., 2008, 2013) and for SSTs from planktonic foraminiferal assemblages, and Mg/Ca and alkenone paleothermometry (Dowsett et al., 2010, 2013; Schreck et al., 2013; Knies et al., 2014).

Data sites north of 60°N provide the focus for this paper, as this is where the significant warming is observed in model simulations. Howell et al. (2014) focus on just six data sites, three marine and three terrestrial, as temperature changes are small at all other sites. This paper extends the focus of the DMC to all data sites north of 60°N where the proxy data temperature estimate exceeds the mean annual temperature from the control simulation. Locations of the sites are shown in Fig. 1.

In addition to the sites used in Howell et al. (2014), mid-Pliocene Arctic SST estimates from Schreck et al. (2013) and Knies et al. (2014), are included. The SST estimate for ODP 911 from Robinson (2009) is not included in this paper, as a newer age model presented by Mattingsdal et al. (2014) put the samples outside the mPWP. The terrestrial site Ocean Point (Nelson and Carter, 1985) is not included in this paper as age estimates for the site

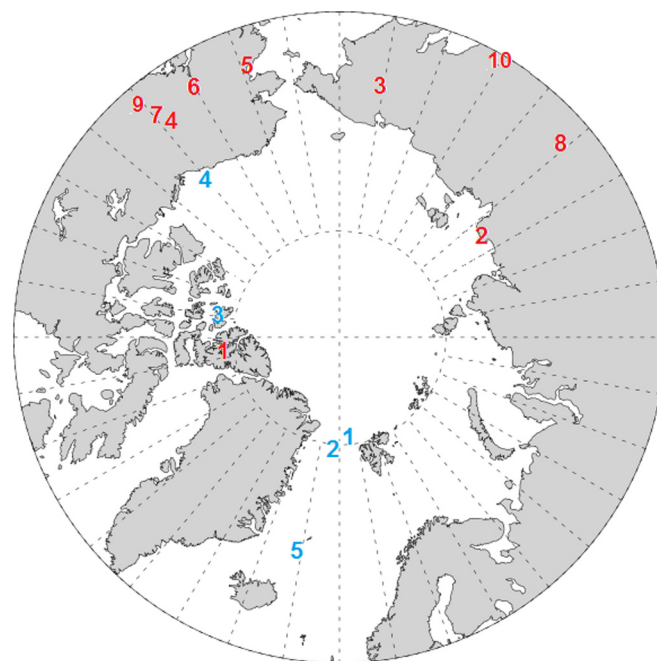


Fig. 1. Location of marine (blue) and terrestrial (red) data sites. Marine data sites: 1. ODP 910C, 2. ODP 909C, 3. Meighen Island, 4. Colvillian, 5. ODP 907A. Terrestrial data sites: 1. Beaver Pond, 2. Lena River, 3. Lake El'gygytyn, 4. Alaska Circle, 5. Blizkiy, 6. Nenana Valley, 7. Lost Chicken Mine, 8. Delyankir, 9. Bonanza Creek, 10. Magadan District. (For interpretation of the references to colour in this figure legend, the reader is referred to the web version of this article.)

are 2.7–2.6 Myr ago, and so is outside the mPWP. A recent mid-Pliocene SAT estimate from Pound et al. (2015) is added to the terrestrial data–model comparison.

The data–model comparison will focus on the difference between the proxy data estimates and the highest mean annual temperature in the ensemble at each data site. In addition to the mean annual temperature, the highest monthly temperature increase in the ensemble at each data site will be shown.

2.3.2. Energy balance analysis

This paper uses the methods set out in Hill et al. (2014) to determine the breakdown of contribution to high latitude SAT changes in selected simulations, enabling an analysis of the differences in patterns of temperature and sea ice changes resulting from the different forcing changes.

3. Results

3.1. Sea ice

3.1.1. Sea ice extent

Twenty-three of the simulations produce a smaller mean annual sea ice extent than the control simulation (Mod_400_0.5, 10.61×10^6 km²), with six producing greater mean annual extents (all five simulations with 300 ppm pCO₂ and standard albedo, and Mar_400_0.5). The annual sea ice extent cycles for each of the 30 simulations are displayed in Fig. 2.

The effects of changing only the orbital configurations from the PlioMIP experimental design are shown in Fig. 2(c), which includes the control simulation, Mod_400_0.5. Compared to the control, the mean annual extent is greater in Mar_400_0.5, and smaller for the other three orbits. Of these, Jul_400_0.5 simulates the smallest mean annual extent (8.92×10^6 km², a decrease of 15.9% compared to the control).

The September sea ice extent minimum simulated by Jul_400_0.5 (Fig. 2(c)) is 0.37×10^6 km², which meets the crite-

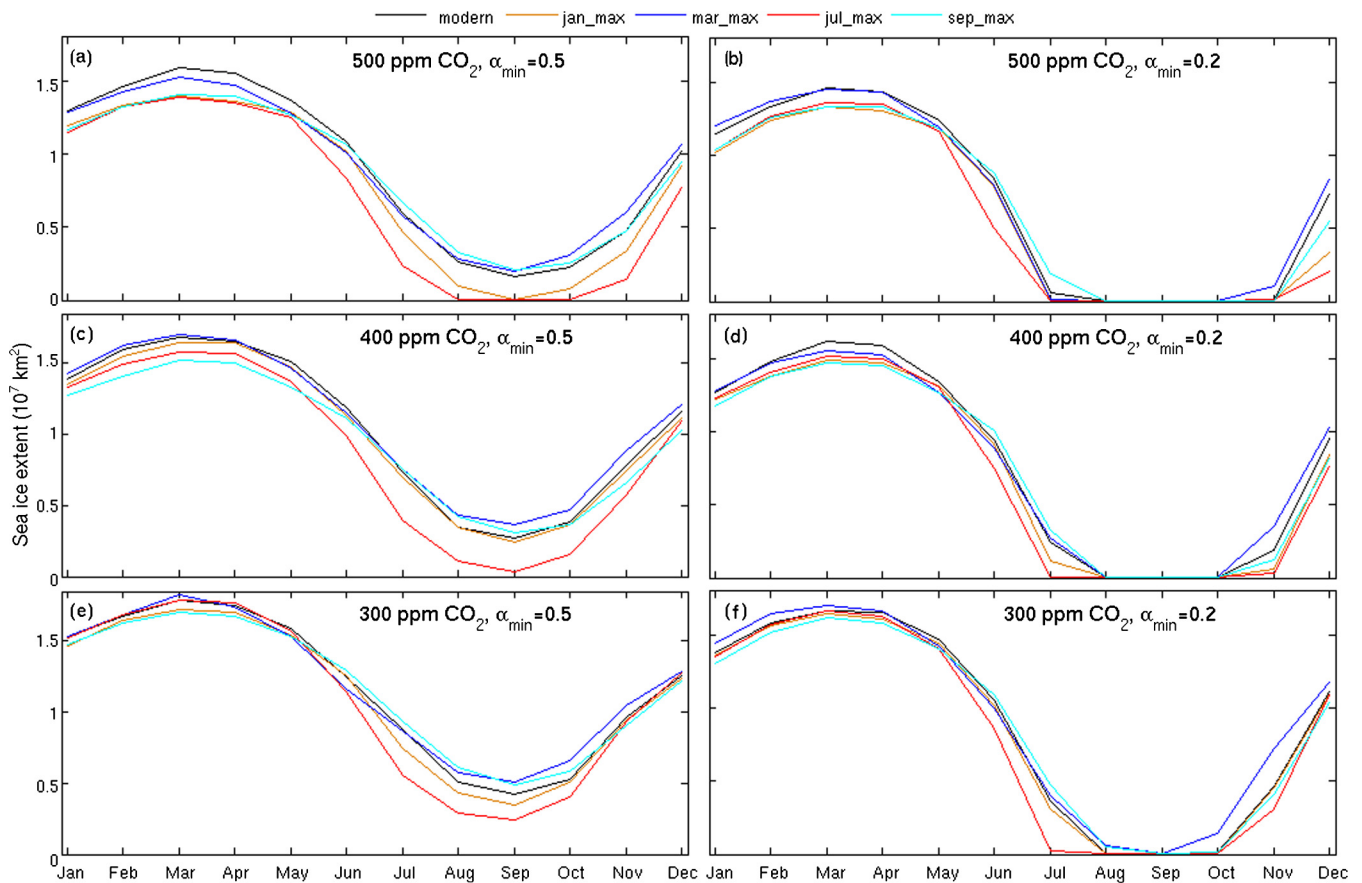


Fig. 2. Annual sea ice extent (10^7 km^2) cycle for all 30 ensemble members. Each panel shows the five orbital simulations with the same $p\text{CO}_2$ and minimum albedo combinations. The only difference between simulations in any given panel is the orbital configuration used.

ria for ‘sea ice free’ conditions of less than 10^6 km^2 (e.g. Wang and Overland, 2009). This demonstrates that a change in orbital configuration only from the control is sufficient to simulate sea ice free conditions in the mid-Pliocene (using the HadCM3 model).

Raising the atmospheric CO_2 levels to 500 ppm (Fig. 2(a, b)) results in a decline in sea ice in every month for all five orbits. In each simulation, the largest reduction occurs in November. From August to September, both the Jan_500_0.5 and Jul_500_0.5 simulations produce a sea ice free Arctic, but the extent in the Mod_500_0.5 simulation does not fall below $1.62 \times 10^6 \text{ km}^2$. Reduction of the atmospheric CO_2 concentration to 300 ppm (Fig. 2(e, f)) has the effect of an increase in sea ice extent in every month, with none of the simulations in this scenario producing sea ice-free months.

Reducing minimum albedo to 0.2 also causes a decrease in sea ice extent in each month of every orbital simulation, compared to the same orbit under standard conditions. All five simulations produce no sea ice from August to October, with the Jul_400_0.2 simulation also producing no sea ice in July. With atmospheric CO_2 levels at 300 ppm and reduced minimum albedo, all simulations produce months with an ice-free Arctic, but have a more rapid sea ice growth in November and December compared to the 400 ppm simulation. Increasing the atmospheric CO_2 to 500 ppm with reduced minimum albedo results in a longer ice-free Arctic period in most of the simulations, and a slower recovery in November and December.

The mean annual change in sea ice extent is $2.11 \times 10^6 \text{ km}^2$ (19.9%). The main driver of this is summer sea ice extent, which sees a mean change of $2.35 \times 10^6 \text{ km}^2$ (69.4%), contrasting to a mean winter change of just $1.46 \times 10^6 \text{ km}^2$ (8.9%).

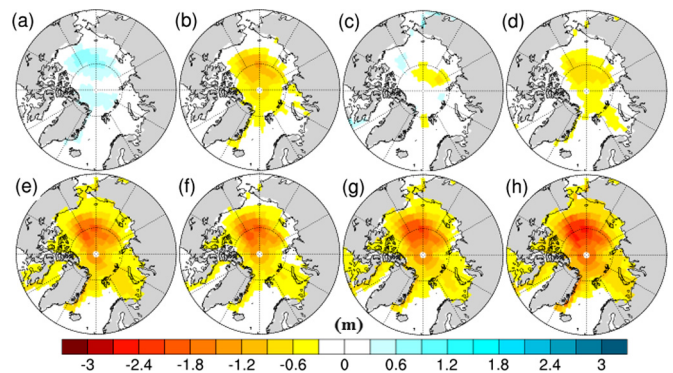


Fig. 3. Mean annual sea ice thickness (m) anomaly (alternative minus control) for simulations: (a) Mar_400_0.5, (b) Jul_400_0.5, (c) Jul_300_0.5, (d) Mod_500_0.5, (e) Jul_500_0.5, (f) Mod_400_0.2, (g) Mod_500_0.2, (h) Jul_500_0.2. Control simulation is Mod_400_0.5.

3.1.2. Sea ice thickness

Twenty-three simulations produce a thinner mean annual sea ice cover (north of 80°N) in comparison to the control simulation (Mod_400_0.5), the same number of simulations that showed a decline in mean annual extent. Fig. 3 shows mean annual thickness anomalies for eight of the simulations (chosen to display the range of different changes in sea ice thickness, SAT (Fig. 4) and SST (Fig. 5), plots for all simulations shown in supplementary information). In all simulations, the change in mean annual thickness is the same sign as the change in mean annual extent, with two exceptions (Sep_400_0.5 simulation simulates a thicker ice cover, despite also simulating a reduced extent, and Jul_300_0.5 simulates thinner than control sea ice, in addition to a greater extent).

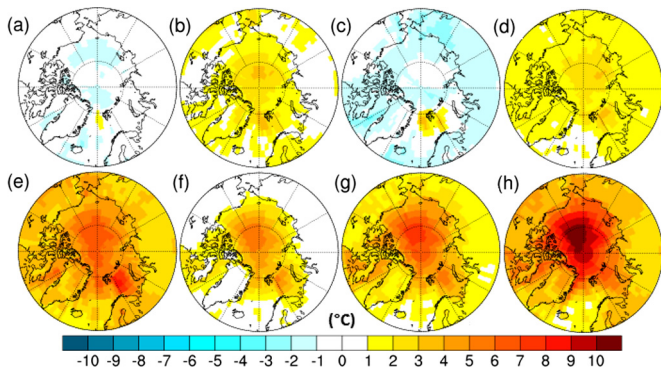


Fig. 4. Mean annual SAT ($^{\circ}\text{C}$) anomaly (alternative minus control) for simulations: (a) Mar_400_0.5, (b) Jul_400_0.5, (c) Jul_300_0.5, (d) Mod_500_0.5, (e) Jul_500_0.5, (f) Mod_400_0.2, (g) Mod_500_0.2, (h) Jul_500_0.2. Control simulation is Mod_400_0.5.

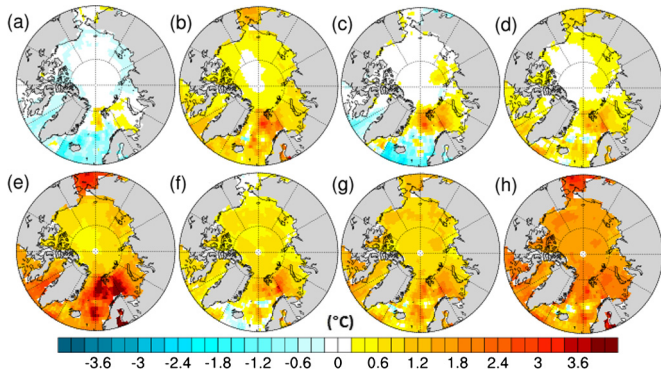


Fig. 5. Mean annual SST ($^{\circ}\text{C}$) anomaly (alternative minus control) for simulations: (a) Mar_400_0.5, (b) Jul_400_0.5, (c) Jul_300_0.5, (d) Mod_500_0.5, (e) Jul_500_0.5, (f) Mod_400_0.2, (g) Mod_500_0.2, (h) Jul_500_0.2. Control simulation is Mod_400_0.5.

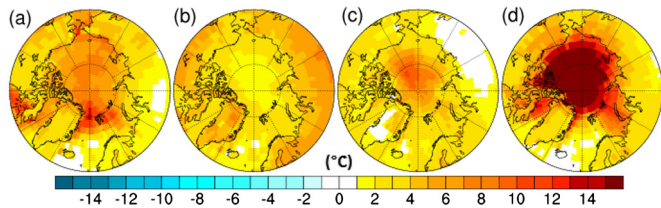


Fig. 6. Seasonal SAT ($^{\circ}\text{C}$) anomalies (compared to control) for the Jul_500_0.2 simulation for (a) FMA, (b) MJJ, (c) ASO, (d) NDJ. Control simulation is Mod_400_0.5.

The change in mean annual sea ice thickness north of 80°N across the ensemble is 0.73 m (34.3%). The mean change in winter is 0.71 m (20.1%), and 0.65 m (72.6%) in summer. The seasonal changes in thickness are far closer in value in comparison to the seasonal changes in extent, although the change of 0.65 m in summer represents a proportionally much greater change from the control than the winter change of 0.71 m.

The simulations with increased atmospheric CO_2 produced less extensive, but thicker winter sea ice in comparison to the simulations with reduced minimum albedo. The mean sea ice thickness north of 80°N thins by an average of 0.54 m in comparison to the control in the increased pCO_2 simulations, whilst the decreased minimum albedo simulations show an average thinning of 0.97 m.

3.2. Temperature changes

3.2.1. Annual and seasonal changes

The large reduction in sea ice seen in many of the simulations has substantial effects on the modelled SATs and SSTs. Feedback

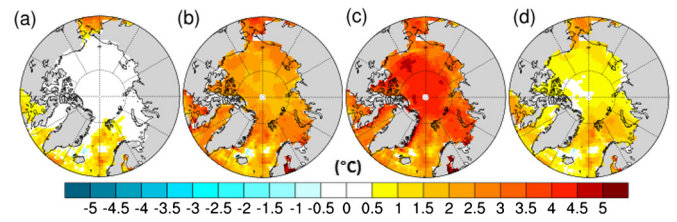


Fig. 7. Seasonal SST ($^{\circ}\text{C}$) anomalies (compared to control) for the Jul_500_0.2 simulation for (a) FMA, (b) MJJ, (c) ASO, (d) NDJ. Control simulation is Mod_400_0.5.

processes mean that reduced sea ice will likely be both a cause of and result of increased temperatures. All but one simulation where the mean annual sea ice extent was reduced in comparison to the control have increases in the mean annual SATs and SSTs north of 60°N . The exception is the Mar_300_0.2 simulation, where the mean annual SAT and SST are reduced, in comparison to the control, by 0.2°C and 0.03°C respectively. Figs. 4 and 5 show mean annual SAT and SST anomalies for eight of the ensemble members, whilst Figs. 6 and 7 show SAT and SST seasonal anomalies for the Jul_500_0.2 simulation.

Changes in SAT are on average greater than changes in SST. For example, as a result of increasing pCO_2 to 500 ppm, the mean annual increase in SST north of 60°N compared to the control is 0.9°C , the equivalent increase in SAT is 2.9°C . The patterns of warming are also different, the largest increases in SST typically occur in July and August, whereas the larger SAT increases are observed in November and December. The SST increase is greatest in summer due to the increase in open water, which would previously have been covered by sea ice. This heat is then released into the atmosphere during the autumn as the sea ice refreezes, producing the large SAT autumn increase. As water has a greater specific heat capacity than air, the overall SST response is smaller than the SAT response. This delayed warming effect and lower SST response have been observed and discussed in previous studies (e.g. Howell et al., 2014; Kumar et al., 2010; Screen and Simmonds, 2010).

The largest increases occur in the simulations with both reduced minimum albedo and increased pCO_2 . The mean annual increase in SST north of 60°N in these simulations is 1.3°C , with a maximum of 1.8°C in the Jul_500_0.2 simulation. The highest mean monthly SST increase is 4.2°C in August in Jul_500_0.2. The mean annual SAT increase north of 60°N in the same five simulations is 4.0°C . Jul_500_0.2 also shows the greatest increase in mean annual SAT, with a rise of 4.8°C , whilst the 9.8°C rise in January in the Jan_500_0.2 simulation is the largest rise in any single month.

Focusing north of 80°N , the SAT changes are even greater. The Jul_500_0.2 mean annual increase is 8.3°C , and the increase in December of the same simulation is 19.8°C . SST increases north of 80°N , however, do not show uniformly higher increases compared to north of 60°N . The mean increase in mean annual SST across the five simulations is 1.1°C , the highest single mean annual change being 1.7°C in Jul_500_0.2. The greatest monthly change is higher, however, with August in Jul_500_0.2 showing an SST increase of 5.0°C compared to the control.

Fig. 8 indicates that the warming north of 60°N from increased pCO_2 is greater than the warming seen in the reduced albedo (400 ppm) simulations (comparing the same orbit), despite there being a smaller reduction in sea ice extent. Whilst this is not also true in all cases when looking at the SST changes, the Jan_500_0.5, Jul_500_0.5 and Sep_500_0.5 simulations with 500 ppm pCO_2 all have higher mean annual SSTs north of 60°N than the same orbital simulations with $\alpha_{\text{min}} = 0.2$.

Table 3

Summary of observational, proxy and modelled temperatures and anomalies at marine data sites. All temperatures are in °C. The mPWP^c simulation is Mod_400_0.5, mPWP^a is Jul_500_0.5 for the ODP sites, and Jul_500_0.2 for the other sites. Column (a) is the data site name and reference. Column (b) is the data site latitude (°N) and longitude (°E) co-ordinates. Column (c) is 20th century (1961–1990) mean annual SST observations from Rayner et al. (2003). Column (d) is proxy-inferred mid-Pliocene mean annual SST. Column (e) is proxy – observation. Column (f) is simulated pre-industrial (PI) mean annual SST. Column (g) is simulated mid-Pliocene control mean annual SST (mPWP^c). Column (h) is warmest ensemble member simulated mid-Pliocene mean annual SST (mPWP^a). Column (i) is mPWP^c – PI. Column (j) is mPWP^a – PI. Column (k) is mPWP^c – proxy. Column (l) is mPWP^a – proxy. Column (m) is percentage change between (k) and (l).

(a)	(b)	(c)	(d)	(e)	(f)	(g)	(h)	(i)	(j)	(k)	(l)	(m)
ODP 907A¹	69.1	2.4	11.7	9.4	3.8	5.5	8.2	1.7	4.2	–6.2	–3.5	43.6
Robinson (2009)	–12.4											
ODP 907A²	69.1	2.4	8.5	6.1	3.8	5.5	8.2	1.7	4.2	–3.0	–0.3	90.0
Schreck et al. (2013)	–12.4											
ODP 909C	78.6	1.1	10.2	9.1	1.5	0.4	3.6	–1.1	2.1	–9.8	–6.6	32.7
Robinson (2009)	–3.1											
ODP 910C	80.2	0.3	4.1	3.8	1.9	0.8	3.3	–1.1	1.4	–3.3	–0.8	75.8
Knies et al. (2014)	6.4											
Colvillian	70.3	–1.5	1.2	2.7	–1.6	–1.0	0.8	0.6	2.4	–2.4	–0.4	83.3
Brouwers (1994)	–150.4											
Meighen Island	79.0	–1.8	1.7	3.5	–1.4	–0.1	1.3	1.3	2.7	–1.8	–0.4	77.8
Fyles et al. (1991)	–99.0											

Table 4

Simulated December (month with largest monthly increase between warmest ensemble member and control) SATs for mid-Pliocene control simulation (mPWP^c, Mod_400_0.5), and warmest ensemble member (mPWP^a, Jul_500_0.2) at terrestrial sites in Table 2. All temperatures in °C. Column (a) is site name. Column (b) is mPWP^c – proxy mean annual temperature anomaly ((k) in Table 2). Column (c) is simulated December SAT in mPWP^c. Column (d) is simulated December SAT in mPWP^a. Column (e) is December mPWP^a – December mPWP^c.

(a)	(b)	(c)	(d)	(e)
Beaver Pond	–14.5	–31.2	–24.2	7.0
Lena River	–12.0	–31.6	–25.4	6.2
Alaska Circle	–5.3	–18.7	–12.1	6.6
Blizkiy	–10.5	–21.9	–17.1	4.8
Nenana Valley	–7.0	–21.4	–14.2	7.2
Lost Chicken Mine	–4.4	–17.4	–11.1	6.3
Bonanza Creek	–8.3	–18.6	–12.0	6.6
Delyankir	–17.0	–33.2	–31.3	1.9
Magadan District	–7.1	–25.5	–22.5	3.0

discrepancy was 4.4 °C at this site. At only one other site, Alaska Circle, is the model-data difference less than 2 °C. At the remaining seven the difference is at least 3 °C, the largest difference being 13.6 °C at Delyankir.

Analysis of pollen assemblages extracted from sediment at Lake El'gygytyn (67.3°N, 172.1°E) suggests that warmest monthly SATs at this location in the mid-Pliocene were approximately 16–17 °C (Brigham-Grette et al., 2013; Andreev et al., 2014). The warmest monthly temperature in the control simulation shows a temperature of 14.4 °C at the location of Lake El'gygytyn, 1.6–2.6 °C cooler than the indications from proxy data. The model fails to achieve the level of warming indicated by the data, as with the mean annual SATs shown in Table 2, but with a smaller temperature discrepancy. Out of the rest of the ensemble, four simulations (Jan_400_0.2, Jul_400_0.2, Jul_300_0.5 and Jul_300_0.2) produced maximum monthly SAT values within the 16–17 °C range, with a further four (Jul_400_0.5, Jan_500_0.5, Jul_500_0.5 and Jul_500_0.2) exceeding this range for warmest monthly mean. As only mean warmest month temperatures were available, Lake El'gygytyn temperatures do not feature in Tables 2 and 4.

Tables 2 and 3 also show the mid-Pliocene warming at each site for data and models, using differences between the proxy data temperatures and 20th century observations of SAT (Legates and Willmott, 1990) and SST (Rayner et al., 2003), and the differences between the simulated mid-Pliocene and pre-industrial temperatures (columns (e) and (i) respectively). The model warming exceeds the data warming only at the Magadan District ter-

Table 5

Simulated August (month with largest monthly increase between warmest ensemble member and control) SSTs for mid-Pliocene control simulation (mPWP^c, Mod_400_0.5), and warmest ensemble member (mPWP^a, Jul_500_0.5) for ODP 907A and ODP 909C, Jul_500_0.2 for the other sites) at sites from Table 3. All temperatures in °C. Column (a) is site name. Column (b) is mPWP^c – proxy mean annual temperature anomaly ((k) in Table 3). Column (c) is August SST in mPWP^c. Column (d) is August SST in mPWP^a. Column (e) is August mPWP^a – August mPWP^c.

(a)	(b)	(c)	(d)	(e)
ODP 907A¹	–6.2	7.7	11.7	4.0
ODP 907A²	–3.0	7.7	11.7	4.0
ODP 909C	–9.8	3.2	7.0	3.8
ODP 910C	–3.3	3.1	6.5	3.4
Colvillian	–2.4	0.5	5.9	5.4
Meighen Island	–1.8	3.7	7.4	3.7

restrial site (by 0.6 °C). The greatest SAT difference is at Delyankir (14.3 °C), whilst the largest SST difference is at ODP 909C (10.2 °C). At ODP sites 909C and 910C, the pre-industrial SSTs are actually warmer than those from the mid-Pliocene simulation (1.5 °C and 1.9 °C compared to 0.4 °C and 0.8 °C respectively, see Table 3). An important caveat to note is that the observations are from the 20th century, so are likely to be warmer than temperatures from the pre-industrial, for which the model simulation comparisons are run.

At six of the terrestrial sites, the SAT increase compared to the control in the warmest ensemble member (Jul_500_0.2) is greater than the difference between the data and model warming at each site. Consequently, the temperature difference between the pre-industrial simulation and Jul_500_0.2 exceeds the difference between the modern observations and the proxy estimates at each site. This shows a degree of agreement between the proxies and the simulation.

Table 4 shows the greatest increase in December SAT (consistently largest SAT increase of all months) in the ensemble from the control, at each terrestrial data site. Out of the nine data sites, the largest monthly change at six of them is smaller than the difference between the mean annual temperature estimates from the proxy data and control simulation. Table 5 shows the greatest increase in August SST (consistently largest SST increase of all months) in the ensemble for each data site. At four sites (ODP 907A², ODP 910C, Colvillian and Meighen Island), the maximum monthly increase exceeds the model–data mean annual anomaly for the control. Only for ODP 907A¹ and ODP 909C would the maximum monthly increase not be enough to close the data–model disparity if it was sustained year-round.

4. Discussion

4.1. Sea ice

Fig. 2(c) indicates that a change in orbital forcing is sufficient to cause the mid-Pliocene Arctic to become ice-free at some point during the summer in HadCM3. In the Jul_400_0.5 simulation, sea ice extent dropped to $0.37 \times 10^6 \text{ km}^2$ in September. However, when the atmospheric CO_2 concentration was also lowered to 300 ppm, no simulation was ice-free at any point. This implies that knowing the atmospheric CO_2 concentration to within 100 ppm is important to ascertaining whether the mid-Pliocene Arctic saw sea ice-free conditions (using HadCM3).

The Jan_500_0.5 simulation achieves ice-free conditions in addition to Jul_500_0.5. Other orbital simulations, notably the standard orbital configuration, do not. This is an important result as it appears to suggest that the Arctic sea ice in the mid-Pliocene is more sensitive to changes that result due to the different orbital configurations than an increase in 100 ppm pCO_2 .

The difference between some simulations producing ice-free conditions under 400 ppm but not under 300 ppm is also an important result, as atmospheric CO_2 during the mPWP is likely to have varied during the period. Based on the results of these simulations, the coinciding of particular orbital configurations with variations in pCO_2 is crucial to whether the Arctic becomes ice-free or not in HadCM3. This suggests that much tighter age control on proxy data will be required in order to make a consistent data-model comparison.

Sea ice-free conditions in the mid-Pliocene Arctic would contradict Darby (2008), who show evidence from iron grains in the ACEX core (located at 87.5°N , -138.3°E) implying that perennial sea ice was present in the Arctic at least as far back as 14 Myr ago. The samples from the core represent approximately 1 ka, sampled at an average rate through the core of 0.17 Ma (± 0.35). It is possible that there were sea ice-free events during the mid-Pliocene which were missed by the sampling, although Darby (2008) asserts that the probability of each of the 155 ACEX samples missing a time where seasonal ice was present is low. The presence of the sea ice proxy IP_{25} (Belt et al., 2007; Brown et al., 2014) in mid-Pliocene sediment from ODP 910C shown in Knies et al. (2014), indicates perennial sea ice conditions at 80°N in the Atlantic sector of the mid-Pliocene Arctic Ocean.

When minimum albedo is reduced to 0.2, the orbital configuration is less significant, as the sea ice disappears completely in each simulation from August to October. This implies that if this is an appropriate parameterisation within HadCM3 for the mPWP, the orbital configuration is less relevant in relation to the issue of the Arctic being ice-free, although it still makes a difference to the timing and duration of the ice-free conditions. The Jan_400_0.2 and Jul_400_0.2 simulations have faster declines from June to July, and slower recoveries after October, which is likely to have an effect on the surface temperatures. Even under 300 ppm pCO_2 , all simulations produce ice-free conditions, with the main effect of the lower pCO_2 appearing to be facilitating a faster sea ice recovery in the winter. Increasing to 500 ppm pCO_2 extends the period of time over which the ice-free summer conditions exist, and slows down the winter recovery.

An important caveat in any assessment of the sensitivity of simulated Arctic sea ice is that conclusions are based on the assumption that HadCM3 is able to simulate mid-Pliocene sea ice well. Howell et al. (2015) suggested that, based on the limited proxy data evidence regarding Pliocene Arctic sea ice, that HadCM3 had the closest agreement with the conclusions of the data in its mPWP simulation of all the PlioMIP models, although other models' CMIP5 sea ice simulations matched modern observations more closely (Shu et al., 2015).

Within the PlioMIP ensemble, HadCM3 was not one of the four models which simulated an ice-free Arctic summer, but did have the lowest summer extent of the four simulations which maintained ice year-round (Howell et al., 2015). In light of the sensitivity which HadCM3 displays with regard to orbit, atmospheric CO_2 and albedo parameterisation, similar assessments of other models, both with summer sea ice and without, would provide interesting insights.

4.2. Temperatures

Using CAM3, an atmosphere-only model, Ballantyne et al. (2013) ran a simulation of the mPWP where Arctic sea ice is absent year round, and showed warming of 10°C to 15°C extending into the continental interior. Subsequently a much closer, although not complete, agreement with proxy data SAT estimates than the control simulation was achieved. However, as stated in Ballantyne et al. (2013), a complete absence of sea ice is not likely to be a realistic mid-Pliocene boundary condition. The ensemble simulations with the highest sea ice reduction (Fig. 2(b)) produce sea ice-free conditions for almost half the year, but by March the extent has recovered to 82.4% of the control value, albeit with a 38.2% drop in mean thickness.

A fully coupled GCM can not maintain the latent heat transfer from ocean to atmosphere throughout the year that is seen in the atmosphere only simulation of Ballantyne et al. (2013), which appears to be required to provide a consistent level of temperature increase in order to close the data-model mismatch. Even if the temperature increases at each site in December were replicated in all other months, this would not be sufficient to produce agreement between models and proxy data temperatures at more than half the terrestrial sites (Table 4).

At the marine sites, the data-model SST difference is less than 1°C for all but ODP 907A¹ and ODP 909C. In the warmest simulation at these two sites (Jul_500_0.5), the data-model difference is 3.5°C and 6.6°C respectively. If the maximum monthly SST increase compared to the control (August) were maintained year-round, the data-model difference would reduce to 2.2°C and 6.0°C respectively. Differences between models and the SST estimates for these sites from Robinson (2009) remain, in contrast to the closer agreement with the more recent SST estimates in Schreck et al. (2013) and Knies et al. (2014) at similar locations.

The discrepancy is lower when comparing the temperature increases for models and data, as opposed to just the temperatures, and at some sites the model warming in some ensemble members is close to or exceeds the data warming. However, at three terrestrial and four marine sites, the model warming is still lower than the data warming, even in the warmest simulations.

A caveat that must be considered when comparing the model and proxy temperatures is that as the proxy data covers 3.3 to 3.0 Myr ago (with wider temporal ranges in the terrestrial data), the samples used may not all be exactly the same age. Expecting the models to achieve the desired level of warming at all sites under the same combination of boundary conditions may not be realistic. The influence that the orbit has on simulated temperatures also questions the value of a comparison of a simulation with a proxy estimate representing the average of several different orbital forcings.

The simulations with atmospheric CO_2 increased to 500 ppm have higher SATs than the simulations with α_{min} reduced to 0.2 in most months, but larger sea ice extents (Figs. 2, 8). The breakdown of the different contributions to high latitude warming is shown in Fig. 9. Clear sky albedo is the dominant contributor in the $\alpha_{\text{min}} = 0.2$ simulations, coming as a result of the change to the albedo parameterisation and subsequent exposure of greater areas of open water as more ice melts, which will then lead to temperature increases.

Greenhouse gas emissivity is, marginally ahead of clear sky albedo, the largest contributor to warming in the 500 ppm simulations. In these runs, the higher atmospheric CO₂ concentrations lead to higher temperatures, which leads to melting sea ice. Feedbacks will enhance both sea ice melt and warming in both sets of simulations. However, in the $\alpha_{min} = 0.2$ runs, it is initial reductions in sea ice which then drive temperature increases, whilst the reverse is the case in the 500 ppm pCO₂ simulations.

In the Mod_400_0.2 simulation, cloud albedo contributed up to 4°C of cooling at high latitudes compared to the control simulation (Fig. 9). The Mod_500_0.5 simulation showed a much lower cooling contribution due to cloud albedo effects at high latitudes in Mod_400_0.2, and other simulations with reduced minimum albedo. The overall surface albedo north of 60°N is lower in Mod_400_0.2 compared to Mod_500_0.5, due to the reduced sea ice in Mod_400_0.2. Consequently, the presence of clouds at high latitudes increases the planetary albedo more in Mod_400_0.2 than in Mod_500_0.5. The difference in the cloud albedo contributions in the energy balance analysis reflect this.

As the results shown in Fig. 8 indicate, changes to the model that directly reduce sea ice, such as the changes made to sea ice albedo, do result in greater high latitude temperatures, but do not appear to be as effective as changes which have a more direct impact on temperature changes, such as atmospheric CO₂ increases. This suggests it may be difficult to achieve the large temperature increases necessary to significantly reduce the data–model disagreements through model adjustments which only indirectly lead to higher temperatures. Alternatively, if models cannot simulate sufficiently warm mean annual temperatures at the proxy data locations, even with significant forcings at high latitudes, then the possibility that the temperatures inferred from proxy data relate to maximum or growing season temperatures, as opposed to mean annual seems more likely.

5. Conclusions

The results in this paper emphasise the uncertainty with regards to the state of sea ice in the mid-Pliocene Arctic. Howell et al. (2015) demonstrated the range of summer sea ice extents from various models, whilst these results show that forcing uncertainties are sufficient, in the simulation of HadCM3, to make a difference between seasonal and perennial sea ice coverage. Results seen in this paper and Howell et al. (2015) give a wide range of potential states of mid-Pliocene Arctic sea ice cover derived from multiple climate models. This demonstrates the need for greater coverage of sea ice proxy data for the mid-Pliocene, which can help to identify the most suitable model and forcing combination which reflects the state of sea ice best. Orbital sensitivity to sea ice cover suggests that it may be difficult. If the sea ice cover in the mid-Pliocene moved between seasonal and perennial coverage depending on the orbital configuration, then the proxy information would have to be highly constrained in time to identify these changes.

Given the effect on the SATs and SSTs which are associated with the variations in sea ice cover, the ability to more accurately constrain the sea ice conditions in the mid-Pliocene may also help constrain the resulting high latitude temperature changes. However, it is likely to be difficult to distinguish between the various ice-free scenarios which are seen in the ensemble. Proxy data would need to indicate the timing of the disappearance and freeze-up of the sea ice, or give an indication to other metrics, such as winter thickness, for which no proxy indicator currently exists.

At the terrestrial sites, with the exception of Lost Chicken Mine and Alaska Circle, no simulation was able to reduce the data–model discrepancies for mean annual temperature estimates to less than 3°C, with some discrepancies still exceeding 8°C. Modelled and proxy SSTs showed closer agreement, with model temperatures less than 1°C lower than four of the six proxy SSTs in

Table 3. Uncertainties associated with the temperature reconstructions are specified for some terrestrial data sites (Salzmann et al., 2013; Pound et al., 2015). With the exception of Bonanza Creek, none of the alternative anomalies in Table 2 are less than any of the given uncertainties. Errors associated with the SST reconstruction methods are less than 2°C (Dowsett et al., 2009), so four of the alternative anomalies in Table 3 are within the uncertainties. The effect of even a very dramatic reduction in the total sea ice cover is not capable of producing agreement at many sites.

As suggested in Ballantyne et al. (2013), a year-round absence of sea ice is perhaps the only way that such high temperature increases can be maintained throughout the year in order to get close agreement between models and data. However, there is evidence for the presence of mid-Pliocene Arctic sea ice (e.g. Darby, 2008; Polyak et al., 2010; Knies et al., 2014), and maintaining ice-free conditions in a coupled AOGCM would require a source of heat into the Arctic during the winter months to prevent freeze-up until the spring. A severely depleted, but not absent, winter sea ice cover might allow for sufficient temperature increase to reduce the data–model mismatch. It is clear from the results of this study that if there is to be closer agreement between proxy and model temperatures, then even the dramatic reductions in sea ice seen in this study will not be sufficient, although they can play an important role in reducing the differences between proxy data and model results. Increased spatial coverage and understanding of the proxy data is crucial to ensure optimal comparison of model and proxy temperatures in the mid-Pliocene.

Acknowledgements

F.W. Howell acknowledges NERC for the provision of a doctoral training grant. F.W. Howell and A.M. Haywood acknowledge that the research leading to these results has received funding from the European Research Council under the European Union's Seventh Framework Programme (FP7/2007–2013)/ERC grant agreement no. 278636. H.J. Dowsett acknowledges funding from the USGS Climate Research and Development (Climate R&D) Program. A.M. Dolan is acknowledged for providing access to the orbital forcing calculations and files. D.J. Hill is acknowledged for providing the code for the energy balance calculations. We thank two anonymous reviewers for their helpful comments and suggestions.

Appendix A. Supplementary material

Supplementary material related to this article can be found online at <http://dx.doi.org/10.1016/j.epsl.2016.02.036>.

References

- Ager, T.A., Matthews, J.V., Yeend, W., 1994. Pliocene terrace gravels of the ancestral Yukon River near Circle, Alaska: palynology, paleobotany, paleoenvironmental reconstruction and regional correlation. *Quat. Int.* 22, 185–206.
- Andreev, A.A., Tarasov, P.E., Wennrich, V., Raschke, E., Herzschuh, U., Nowaczyk, N.R., Brigham-Grette, J., Melles, M., 2014. Late Pliocene and early Pleistocene vegetation history of northeastern Russian Arctic inferred from the Lake El'gygytyn pollen record. *Clim. Past* 10 (3), 1017–1039.
- Badger, M., Schmidt, D., Mackensen, A., Pancost, R., 2013. High-resolution alkenone palaeobarometry indicates relatively stable pCO₂ during the Pliocene (3.3–2.8 Ma). *Philos. Trans. R. Soc. Lond. Ser. A, Math. Phys. Sci.* 68, 20130094.
- Ballantyne, A., Axford, Y., Miller, G., Otto-Bliesner, B., Rosenbloom, N., White, J., 2013. The amplification of Arctic terrestrial surface temperatures by reduced sea-ice extent during the Pliocene. *Palaeogeogr. Palaeoclimatol. Palaeoecol.* 386, 59–67.
- Ballantyne, A., Greenwood, D., Damste, J., Csank, A., Eberle, J., Ryczbyski, N., 2010. Significantly warmer Arctic surface temperatures during the Pliocene indicated by multiple independent proxies. *Geology* 38 (7), 603–606.
- Belt, S., Masse, G., Rowland, S., Poulin, M., Michel, C., LeBlanc, B., 2007. A novel chemical fossil of palaeo sea ice: IP₂₅. *Org. Geochem.* 38 (1), 16–27.
- Brigham-Grette, J., Melles, M., Minyuk, P., Andreev, A., Tarasov, P., DeConto, R., Koenig, S., Nowaczyk, N., Wennrich, V., Rosén, P., Haltia, E., Cook, T., Gebhardt,

- C., Meyer-Jacob, C., Snyder, J., Herzsich, U., 2013. Pliocene warmth, polar amplification, and stepped Pleistocene cooling recorded in NE Arctic Russia. *Science* 340 (6139), 1421–1427.
- Brouwers, E.M., 1994. Late Pliocene paleoecologic reconstructions based on ostracode assemblages from the Sagavanirktok and Gubik formations, Alaskan North Slope. *Arctic* 47, 16–33.
- Brown, T., Belt, S., Tatak, A., Mundy, C., 2014. Source identification of the Arctic sea ice proxy IP_{25} . *Nat. Commun.* 5 (3).
- Bryan, K., 1969. Climate and the ocean circulation III. The ocean model. *Mon. Weather Rev.* 97, 806–827.
- Cattle, H., Crossley, J., 1995. Modeling Arctic climate change. *Philos. Trans. R. Soc. A, Math. Phys. Eng. Sci.* 352 (1699), 201–213.
- Cox, P., Betts, R., Bunton, C., Essery, R., Rowntree, P., Smith, J., 1999. The impact of new land surface physics on the GCM simulation of climate and climate sensitivity. *Clim. Dyn.* 15 (3), 183–203.
- Cronin, T.M., Whatley, R., Wood, A., Tsukagoshi, A., Ikeya, N., Brouwers, E.M., Briggs, W.M., 1993. Microfaunal evidence for elevated Pliocene temperatures in the Arctic ocean. *Paleoceanography* 8 (2), 161–173.
- Curry, J.A., Schramm, J.L., Ebert, E.E., 1995. Sea ice-albedo climate feedback mechanism. *J. Climate* 8 (2), 240–247.
- Darby, D.A., 2008. Arctic perennial ice cover over the last 14 million years. *Paleoceanography* 23, PA1507.
- Dowsett, H., Foley, K., Stoll, D., Chandler, M., Sohl, L., Bentsen, M., Otto-Bliesner, B., Bragg, F., Chan, W.-L., Contoux, C., Dolan, A., Haywood, A., Jonas, J., Jost, A., Kamae, Y., Lohmann, G., Lunt, D., Nisancioglu, K., Abe-Ouchi, A., Ramstein, G., Riesselman, C., Robinson, M., Salzmann, U., Stepanek, C., Strother, S., Ueda, H., Yan, Q., Zhang, Z., 2013. Sea surface temperature of the mid-Piacenzian ocean: a data–model comparison. *Sci. Rep.* 3, 149–163.
- Dowsett, H., Haywood, A., Valdes, P., Robinson, M., Lunt, D., Hill, D., Stoll, D., Foley, K., 2011. Sea surface temperatures of the mid-Piacenzian Warm Period: a comparison of PRISM3 and HadCM3. *Palaeogeogr. Palaeoclimatol. Palaeoecol.* 309 (1–2), 83–91.
- Dowsett, H., Robinson, M., Foley, K., 2009. Pliocene three-dimensional global ocean temperature reconstruction. *Clim. Past* 5 (4), 769–783.
- Dowsett, H.J., Robinson, M.M., Haywood, A.M., Salzmann, U., Hill, D.J., Sohl, L., Chandler, M.A., Williams, M., Foley, K., Stoll, D., 2010. The PRISM3D paleoenvironmental reconstruction. *Stratigraphy* 7 (2–3), 123–139.
- Edwards, J., Slingo, A., 1996. Studies with a flexible new radiation code. 1: Choosing a configuration for a large-scale model. *Q. J. R. Meteorol. Soc.* 122 (531), 689–719.
- Fradkina, A.F., 1991. In: Thompson, R.S., Borisoka, O.K., Svetitskaya, T.V. (Eds.), Abstracts of the Joint US/USSR Workshop on Pliocene Palaeoclimates, p. 22.
- Fyles, J., Marinovich Jr., L., Matthews Jr., J., Barendregt, R., 1991. Unique mollusc find in the Beaufort Formation (Pliocene) on Meighen Island, Arctic Canada. *Curr. Res., Part B, Geol. Surv. Can.*, 105–112. Paper 91.
- Gordon, C., Cooper, C., Senior, C.A., Banks, H., Gregory, J.M., Johns, T.C., Mitchell, J.F.B., Wood, R.A., 2000. The simulation of SST, sea ice extents and ocean heat transports in a version of the Hadley Centre coupled model without flux adjustments. *Clim. Dyn.* 16 (2–3), 147–168.
- Gregory, D., Shutts, G., Mitchell, J., 1998. A new gravity-wave-drag scheme incorporating anisotropic orography and low-level wave breaking: impact upon the climate of the UK Meteorological Office Unified Model. *Q. J. R. Meteorol. Soc.* 124 (546), 463–493.
- Haywood, A., Valdes, P., 2004. Modelling Pliocene warmth: contribution of atmosphere, oceans and cryosphere. *Earth Planet. Sci. Lett.* 218 (3–4), 363–377.
- Haywood, A.M., Dowsett, H.J., Robinson, M.M., Stoll, D.K., Dolan, A.M., Lunt, D.J., Otto-Bliesner, B.L., Chandler, M.A., 2011. Pliocene Model Intercomparison Project (PlioMIP): experimental design and boundary conditions (Experiment 2). *Geosci. Model Dev.* 4 (3), 571–577.
- Haywood, A.M., Hill, D.J., Dolan, A.M., Otto-Bliesner, B.L., Bragg, F.J., Chan, W.L., Chandler, M.A., Contoux, C., Dowsett, H.J., Jost, A., Kamae, Y., Lohmann, G., Lunt, D.J., Abe-Ouchi, A., Pickering, S.J., Ramstein, G., Rosenbloom, N.A., Salzmann, U., Sohl, L., Stepanek, C., Ueda, H., Yan, Q., Zhang, S.Z., 2013. Large-scale features of Pliocene climate: results from the Pliocene Model Intercomparison Project. *Clim. Past* 9 (1), 191–209.
- Hibler, W.D., 1979. A dynamic–thermodynamic sea ice model. *J. Phys. Oceanogr.* 9, 815–846.
- Hill, D.J., Haywood, A.M., Lunt, D.J., Hunter, S.J., Bragg, F.J., Contoux, C., Stepanek, C., Sohl, L., Rosenbloom, N.A., Chan, W.L., Kamae, Y., Zhang, Z., Abe-Ouchi, A., Chandler, M.A., Jost, A., Lohmann, G., Otto-Bliesner, B.L., Ramstein, G., Ueda, H., 2014. Evaluating the dominant components of warming in Pliocene climate simulations. *Clim. Past* 10 (1), 79–90.
- Howell, F.W., Haywood, A.M., Dolan, A.M., Dowsett, H.J., Francis, J.E., Hill, D.J., Pickering, S.J., Pope, J.O., Salzmann, U., Wade, B.S., 2014. Can uncertainties in sea ice albedo reconcile patterns of data–model discord for the Pliocene and 20th/21st centuries? *Geophys. Res. Lett.* 41 (6), 2011–2018.
- Howell, F.W., Haywood, A.M., Otto-Bliesner, B.L., Bragg, F., Chan, W.-L., Chandler, M.A., Contoux, C., Kamae, Y., Abe-Ouchi, A., Rosenbloom, N.A., Stepanek, C., Zhang, Z., 2015. Arctic sea ice in the PlioMIP ensemble: is model performance for modern climates a reliable guide to performance for the past or the future? *Clim. Past Discuss.* 11 (2), 1263–1312.
- Kellogg, W., 1975. Climatic feedback mechanisms involving the polar regions. In: *Climate of the Arctic*, pp. 111–116.
- Knies, J., Cabedo-Sanz, P., Belt, S.T., Baranwal, S., Fietz, S., Rosell-Melé, A., 2014. The emergence of modern sea ice cover in the Arctic Ocean. *Nat. Commun.* 5, 5608.
- Kumar, A., Perlwitz, J., Eischeid, J., Quan, X., Xu, T., Zhang, T., Hoerling, M., Jha, B., Wang, W., 2010. Contribution of sea ice loss to Arctic amplification. *Geophys. Res. Lett.* 37.
- Laskar, J., Robutel, P., Joutel, F., Gastineau, M., Correia, A., Levrard, B., 2004. A long-term numerical solution for the insolation quantities of the Earth. *Astron. Astrophys.* 428, 261–285.
- Legates, D., Willmott, C., 1990. Mean seasonal and spatial variability in global surface air temperature. *Theor. Appl. Climatol.* 41, 11–21.
- Mattingsdal, R., Knies, J., Andreassen, K., Fabian, K., Husum, K., Grøsfjeld, K., Schepfer, S.D., 2014. A new 6 Myr stratigraphic framework for the Atlantic–Arctic gateway. In: *Arctic Palaeoclimate and Its Extremes*. *Quat. Sci. Rev.* 92, 170–178.
- Maykut, G., 1978. Energy exchange over young sea ice in the central Arctic. *J. Geophys. Res.*, Oceans 83 (C7), 3646–3658.
- Maykut, G., Untersteiner, N., 1971. Some results from a time-dependent thermodynamic model of sea ice. *J. Geophys. Res.* 76 (6), 1550–1575.
- Moran, K., Backman, J., Brinkhuis, H., Clemens, S.C., Cronin, T., Dickens, G.R., Eynaud, F., Gattacceca, J., Jakobsson, M., Jordan, R.W., Kaminski, M., King, J., Koc, N., Krylov, A., Martinez, N., Matthiessen, J., McInroy, D., Moore, T.C., Onodera, J., O'Regan, M., Pälike, H., Rea, B., Rio, D., Sakamoto, T., Smith, D.C., Stein, R., St John, K., Suto, I., Suzuki, N., Takahashi, K., Watanabe, M., Yamamoto, M., Farrell, J., Frank, M., Kubik, P., Jokat, W., Kristoffersen, Y., 2006. The Cenozoic palaeoenvironment of the Arctic Ocean. *Nature* 441 (7093), 601–605.
- Nelson, R.E., Carter, L., 1985. Pollen analysis of a Late Pliocene and Early Pleistocene section from the Gubik Formation of Arctic Alaska. *Quat. Res.* 24 (3), 295–306.
- Pagani, M., Liu, Z., LaRiviere, J., Ravelo, A.C., 2010. High Earth-system climate sensitivity determined from Pliocene carbon dioxide concentrations. *Nat. Geosci.* 3 (1), 27–30.
- Perovich, D., Polashenski, C., 2012. Albedo evolution of seasonal Arctic sea ice. *Geophys. Res. Lett.* 39.
- Polyak, L., Alley, R.B., Andrews, J.T., Brigham-Grette, J., Cronin, T.M., Darby, D.A., Dyke, A.S., Fitzpatrick, J.J., Funder, S., Holland, M.M., Jennings, A.E., Miller, G.H., O'Regan, M., Savelle, J., Serreze, M., St John, K., White, J.W.C., Wolff, E., 2010. History of sea ice in the Arctic. *Quat. Sci. Rev.* 29 (15–16), 1757–1778.
- Popova, S., Utescher, T., Gromyko, D., Bruch, A.A., Mosbrugger, V., 2012. Palaeoclimate evolution in Siberia and the Russian Far East from the Oligocene to Pliocene – evidence from fruit and seed floras. *Turk. J. Earth Sci.* 21, 315–334.
- Pound, M.J., Lowther, R.L., Peakall, J., Chapman, R.J., Salzmann, U., 2015. Palynological evidence for a warmer boreal climate in the Late Pliocene of the Yukon Territory, Canada. *Palynology* 39 (1), 91–102.
- Rayner, N.A., Parker, D.E., Horton, E.B., Folland, C.K., Alexander, L.V., Rowell, D.P., Kent, E.C., Kaplan, A., 2003. Global analyses of sea surface temperature, sea ice, and night marine air temperature since the late nineteenth century. *J. Geophys. Res.*, Atmos. 108 (d14), 4407.
- Riihela, A., Mannien, T., Laine, V., 2013. Observed changes in the albedo of the Arctic sea-ice zone for the period 1982–2009. *Nat. Clim. Change* 3 (10), 895–898.
- Robinson, M., 2009. New quantitative evidence of extreme warmth in the Pliocene Arctic. *Stratigraphy* 6 (4), 265–275.
- Rybczynski, N., Gosse, J.C., Harington, C.R., Wogelius, R.A., Hidy, A.J., Buckley, M., 2013. Mid-Pliocene warm-period deposits in the High Arctic yield insight into camel evolution. *Nat. Commun.* 4, 1550.
- Salzmann, U., Dolan, A., Haywood, A., Chan, W.-L., Voss, J., Hill, D., Abe-Ouchi, A., Otto-Bliesner, B., Bragg, F., Chandler, M., Contoux, C., Dowsett, H., Jost, A., Kamae, Y., Lohmann, G., Lunt, D., Pickering, S., Pound, M., Ramstein, G., Rosenbloom, N., Sohl, L., Stepanek, C., Ueda, H., Zhang, Z., 2013. Challenges in quantifying Pliocene terrestrial warming revealed by data–model discord. *Nat. Clim. Change* 3 (1), 969–974.
- Salzmann, U., Haywood, A., Lunt, D., Valdes, P., Hill, D., 2008. A new global biome reconstruction and data–model comparison for the Middle Pliocene. *Glob. Ecol. Biogeogr.* 17 (3), 432–447.
- Schreck, M., Meheust, M., Stein, R., Matthiessen, J., 2013. Response of marine palynomorphs to Neogene climate cooling in the Iceland Sea (ODP Hole 907A). *Mar. Micropaleontol.* 101, 49–67.
- Screen, J., Simmonds, I., 2010. Increasing fall–winter energy loss from the Arctic Ocean and its role in Arctic temperature amplification. *Geophys. Res. Lett.* 37.
- Seki, O., Foster, G.L., Schmidt, D.N., Mackensen, A., Kawamura, K., Pancost, R.D., 2010. Alkenone and boron-based Pliocene pCO_2 records. *Earth Planet. Sci. Lett.* 292 (1–2), 201–211.
- Semtner, A.J., 1976. A model for the thermodynamic growth of sea ice in numerical investigations of climate. *J. Phys. Oceanogr.* 6, 379–389.
- Shu, Q., Song, Z., Qiao, F., 2015. Assessment of sea ice simulations in the CMIP5 models. *Cryosphere* 9 (1), 399–409.
- Wang, M., Overland, J., 2009. A sea ice free summer Arctic within 30 years? *Geophys. Res. Lett.* 36, L07502.
- Zhang, J., Lindsay, R., Schweiger, A., Steele, M., 2013. The impact of an intense summer cyclone on 2012 Arctic sea ice retreat. *Geophys. Res. Lett.* 40 (4), 720–726.